How mesoscopic staircases condense to macroscopic barriers in confined plasma turbulence

Arash Ashourvan and P. H. Diamond

How Mesoscopic Staircases Condense to Macroscopic Barriers in Confined Plasma Turbulence

Arash Ashourvan and P. H. Diamond

Center for Momentum Transport and Flow Organization,
Center for Energy Research, and
Center for Astrophysics and Space Sciences (CASS) & Department of Physics,
University of California San Diego, La Jolla, CA, 92093

This paper sets forth the mechanism by which mesoscale staircase structures condense to form macroscopic states of enhanced confinement. Density, vorticity and turbulent potential enstrophy (PE) are the variables for this model. Formation of the staircase structures is due to inhomogeneous mixing of (generalized) potential vorticity (PV). Such mixing results in the local sharpening of density and vorticity gradients. When PV gradients steepen, the density staircase structure develops into a lattice of mesoscale 'jumps' and 'steps', which are, respectively, regions of local gradient steepening and flattening. The jumps then merge and migrate in radius, leading to the emergence of new macroscale profile structure, so indicating that profile self-organization is a *global* process, which may be described by a local, but nonlinear model. This work is the first to predict and demonstrate how mesoscale condensation of staircases leads to global states of enhanced confinement.

A feature common to self-organizing, nonequilibrium nonlinear systems is the formation of patterns. Patterns of mixed layers, observed in the ocean [1], emerge from double-diffusive convective instability and salt fingering [2–4]. In the turbulent gas of planetary atmospheres, pattern formation manifests itself by the formation of quasi-periodic flow patterns, such as the lateral belts in the Jovian atmosphere [5, 6]. In magnetized plasmas, E×B zonal flow (ZF) shear patterns develop from drift-wave (DW) turbulence. ZFs are also a topic of interest to the magnetic fusion community due to their important role in regulating turbulent transport and triggering the development of the H-mode and internal transport barriers (ITBs) [7–9] (see Refs. 10 and. 11 for a general review of the zonal flows). Recently Ref. 12 reported the observation of a new class of quasi-periodic 'E×B staircase' flow patterns in gyrokinetic simulations. There, E×B staircases formed spontaneously, were self-organizing, and had a long lifespan. Moreover, ∇T_i corrugations coincided with these flow staircase jumps, while in-between the shear layers, turbulent avalanching [14–16] persisted. Furthermore, Ref. 13 reported the experimental evidence for coherent shearing-turbulence modulational states in the Tore Supra tokamak. These results are consistent with interpretation as an E × B staircase, though much more data is required to make a conclusive identification. These observations motivate the search for a reduced model which can explain the underlying mechanism generating these long lasting shear patterns and pressure corrugations.

In a related vein, there have been extensive theoretical studies of ZF generation mechanisms and ZF growth rates, and numerous comparisons to numerical simulations [17]. There has also been some limited progress towards the understanding of collisionless saturation mechanisms for ZFs [17–19]. However, the spatial structure of the zonal shearing fields and their nonlinear evolution in time and space remain poorly understood. Here, we present a theoretical model for the study of space-time flow structure in the context of a simple DW turbulence system. The goal is to better understand two subjects:
1) the evolution and formation of mesoscale density profile staircase structure, and the associated mesoscale shearing lattice pattern, and scales thereof.
2) how a steady *macroscale* transport barrier might emerge from the *mesoscale* density staircase, as a result of a *global* transport bifurcation.

Emergence of shear layers follows from the central idea of positive feedback resulting from inhomogeneous turbulent mixing. This leads to the formation of regions with strong mixing and weak wave elasticity [20] (i.e. memory), separated by interfaces with steepened PV gradients and sharpened flows. The reduced model presented here exhibits both the formation of staircases in the mean density field, similar to buoyancy layering in the *Phillips effect* [21], and also the formation of a mean shear flow lattice pattern, similar to the jet staircase formation in the *PV-Phillips effect* [22]. Hence, this model goes beyond Ref. 23, in that it evolves two coupled mean fields, and turbulent enstrophy density (Ref. 23 evolved only one mean field, the mean buoyancy, and turbulent kinetic energy). Here, cross-correlation of mean fields is addressed self-consistently via the residual stress in the Reynolds stress. In addition, we show that the evolution of the mesoscale density staircase and shear lattice through merger and spatial migration can lead to global transport bifurcation and the formation of macroscale barriers by a sequence of jump mergers and spatial migration.

The reduced model is based on the Hasegawa-Wakatani (HW) system of equations for collisional DW turbulence in a straight magnetic field [24, 25], with electrons in near-adiabatic regime. In this model, conservation of PE and inhomogeneous mixing of PV leads to the spontaneous generation of ZF by turbulence (Reynolds stress). The system variables are functions of time and radius, and consist of mean (reduced) density: $n \equiv \log(N/N_0)$ (N is the particle density and N_0 is a nor-

malization constant), mean vorticity: $u \equiv \rho_s^2 \nabla_\perp^2 (e\phi/T_e)$ ($\rho_s = c(m_i T_e)^{1/2}/eB$), mean PV: $q \equiv n - u$, and the turbulent PE: $\varepsilon \equiv \langle (\delta n - \delta u)^2 \rangle /2$ where δn and δu are respectively the perturbations in density and vorticity, and the averaging is over the directions of symmetry y and z. The set of reduced evolution equations describing the system are given by:

$$\partial_t n = \partial_x D_n \partial_x n + D_c \partial_x^2 n \qquad (1)$$

$$\partial_t u = \partial_x (D_n - \chi) \partial_x n + \chi \partial_x^2 u + \mu_c \partial_x^2 u \qquad (2)$$

$$\partial_t \varepsilon = \partial_x D_\varepsilon \partial_x \varepsilon + \chi [\partial_x (n - u)]^2 - \varepsilon_c^{-1} \varepsilon^{3/2} + \mathcal{P} \qquad (3)$$

The first term in Eq.(1) is the gradient of turbulent particle flux which is given by a local Fickian diffusive term $\Gamma = -D_n \partial_x n$, where D_n is the turbulent particle diffusion coefficient. Both the first and the second term in Eq. (2) come from taking the product of $-\partial_x$ on the turbulent vorticity flux $\Pi = (\chi - D_n) \partial_x n - \chi \partial_x u$, where χ is the turbulent viscosity. The first term in Eq.(2) is the residual stress which is an off diagonal term and can accelerate vorticity due to the basic density gradient. The second term in Eq.(2) is the turbulent viscous diffusion. The terms in Eqs.(1) and (2) which are proportional to μ_u and D_c are respectively the viscosity and diffusivity terms that remove energy from fine scales. In Eq.(3) the term $-\varepsilon_c^{-1} \varepsilon^{3/2}$ is the dissipative term as the result of forward cascade of PE. Furthermore, Fickian diffusive flux form is used for the turbulent flux of PE $\langle \delta v_x \varepsilon \rangle = -D_\varepsilon \partial_x \varepsilon$, where D_ε is the turbulent PE diffusion coefficient. The external turbulence production source in Eq.(3), i.e., $\mathcal{P}$, is due to sources of free energy which are external to the closed system described by the classic DW-HW equations. The production term due to this mechanism, described by the relation $\mathcal{P} = \gamma_\varepsilon \varepsilon$, is linear in ε and is proportional to γ_ε, the characteristic growth of the instabilities responsible for $\mathcal{P}$.

Imposing the condition $\partial_x \varepsilon = 0$ at the boundaries prevents the influx-outflux of turbulent PE. As a result, the system described by the set of Eqs.(1)-(3), manifestly conserves the total PE (sum of mean and turbulent PE), up to damping terms and external forcing. In constructing the reduced turbulence model, mixing length and phenomenological arguments are used to obtain the functional form of the turbulent diffusion coefficients D_n, χ and D_ε. The quasilinear flux relations obtained in Ref. 26, and timescale ordering of $\alpha_n > \omega_m/k_m > $ v are used to approximate D_n and χ. For D_n, the approximation $|k_m \delta \varphi| = |\delta v_x| \approx l \varepsilon^{1/2}$ gives $D_n \approx \frac{k_\perp^2}{1+k_\perp^2} \frac{k_m^2 |\delta \varphi|^2}{\eta k_\parallel^2} \cong l^2 \frac{\varepsilon}{\alpha}$, where the parameter α is identified as the measure of the resistive diffusion rate in the parallel direction: $\alpha = (1 + k_\perp^2)/k_\perp^2 \eta k_\parallel^2$. χ is obtained as: $\chi(x) \cong c_\chi l^2 \varepsilon /\sqrt{\alpha^2 + a_u u^2}$. The term $a_u u^2$ in the denominator incorporates the effect of strong flow shear suppression [27, 28]. The strength of turbulent viscosity (χ) is controlled by c_χ. Moreover, for D_ε the expression $D_\varepsilon(x) \cong \beta l^2 \varepsilon^{1/2}$ is used. Here the parameter β controls the strength of turbulence spreading [29] of PE.

a. *The mixing length:* Inhomogeneous mixing of PV is implemented via a dynamic mixing length, l which is a nonlinear hybrid of two length scales; a constant forcing scale l_0 and the Rhines scale [30], $l_{Rh} = \sqrt{\varepsilon}/|\partial_x (n - u)|$. At the Rhines scale, the turbulence dominated spectral range crosses over to the strongly elastic, wave dominated range. The choice of the functional form of l_{Rh} captures the positive feedback which drives the feature forming instabilities and leads to the formation of nonlinear density staircase and shearing lattice. We employ the following model for the mixing length. [23]:

$$l = \frac{l_0}{(1 + l_0^2 [\partial_x (n - u)]^2/\varepsilon)^{\kappa/2}} \qquad (4)$$

In a system with weak mean PV gradient such that $l_0 < l_{Rh}$, l_0 is the natural choice for the length-scale of turbulent mixing. However, locally the PV gradient of the system can become strong enough such that $l_{Rh} < l_0$ and the mixing length can be approximated by $l \sim l_0^{1-\kappa} l_{Rh}^\kappa$. At these locations of steep PV gradient, l_{Rh} is the governing spatial scale for the turbulence.

Feature forming instabilities result from local transport bifurcations. In the relation between the *local* turbulent flux versus *local* mean gradient (e.g. PV flux $\Gamma_q(x)$ versus PV gradient $\nabla q(x)$) transport bifurcation manifests in the form of an *S-curve*. The *S-curve* consists of two stable mean gradient ranges in which $\delta \Gamma_q/\delta |\nabla q| > 0$, enclosing the region of negative diffusion in which $\delta \Gamma_q/\delta |\nabla q| < 0$. The positive feedback loop in the negative diffusion region drives the instabilities which lead to nonlinear feature formation in the mean profile.

We reduce the number of parameters in the system by the following rescaling choices $x = x/L, t = \gamma_\varepsilon t (l_0/L)^2, \varepsilon = \varepsilon/\gamma_\varepsilon^2, n = n \frac{l_0}{L \gamma_\varepsilon^2}, u = u \frac{l_0}{L \gamma_\varepsilon^2}, l = l/l_0, \alpha = \alpha/\gamma_\varepsilon, \mu_c = \mu_c/(\gamma_\varepsilon l_0^2), a_u = a_u (L/l_0)^2$. The rescaled evolution equations are:

$$\partial_t n = \partial_x \left[\left(\frac{l^2 \varepsilon}{\alpha} \right) \partial_x n \right] + D_c \partial_x^2 n \qquad (5)$$

$$\partial_t u = \partial_x \left[\left(\frac{l^2 \varepsilon}{\alpha} - \frac{c_\chi l^2 \varepsilon}{\sqrt{\alpha^2 + a_u u^2}} \right) \partial_x n \right] + \frac{c_\chi l^2 \varepsilon}{\sqrt{\alpha^2 + a_u u^2}} \partial_x^2 u + \mu_c \partial_x^2 u$$

$$\partial_t \varepsilon = \beta \partial_x \left[l^2 \varepsilon^{1/2} \partial_x \varepsilon \right] + \Lambda \left[\frac{c_\chi l^2 \varepsilon}{\sqrt{\alpha^2 + a_u u^2}} [\partial_x (n - u)]^2 - \frac{\varepsilon^{3/2}}{\varepsilon_c^{1/2}} + \varepsilon \right]$$

where $\Lambda = L^2/l_0^2$. In order to find the parameter ranges in which there is possibility for the growth and formation of structures in density and vorticity profiles, linear analysis is performed on the simple equilibria with uniform density gradient and turbulent PE, and no flow shear.

b. *Numerical solutions of the reduced model* The numerical solutions for the set of nonlinear equations (5) are explored using a finite difference method in space and the Runge-Kutta-Fehlberg method for time integration. Initial conditions are chosen as: $n(x,0) = -g_i x; u(x,0) = 0; \varepsilon(x,0) = \varepsilon_i$. The values g_i, ε_i are obtained from the linearly unstable region of the parameter space. Boundary conditions are $n(0,t) = 0, n(1,t) = -g_i; u(0,t) =$
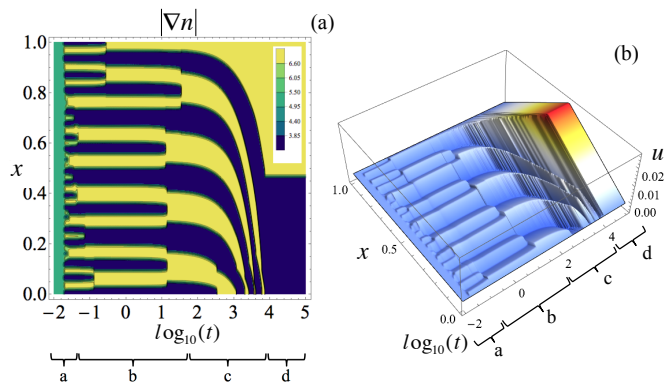
FIG. 1: (2a) Contour plot of the time evolution of $|\nabla n|$ along the plasma radius for
$\Lambda = 4000, c_\chi = 0.95, \alpha = 6, \varepsilon_c = 6.25, \beta = 0.1, \mu_c = D_c = 0.78, a_u = 1, g_i = 5.1, \varepsilon_i = 0.002$. Horizontal axis is the log of time; vertical is the scaled radius. Different stages of evolution are: a) Fast merger of micro-steps and formation of meso-steps. b) Coalescence of meso-steps to barriers. c) Barriers propagate along gradient, condense at boundaries. d) Stationary profile. (2b) Evolutionary landscape of the vorticity profile u(i.e., the shearing profile), as a function of position x and time t.

$u(1,t) = 0$ and $\partial_x \varepsilon(0,t) = \partial_x \varepsilon(1,t) = 0$. Numerical solutions of the system exhibit roughly three stages of evolution 1) development of nonlinear mesoscale features from microscale instabilities 2) evolution of mesoscale structure through local merger processes leading to the formation of mesoscale barriers 3) detachment of the structures from their inception locations and their migration towards the boundaries, resulting in the formation of the steady macroscale structure. Each stage of evolution has a characteristic time-scale and length-scale. Figures 1a and 1b respectively show the evolution landscape of density profile and vorticity profile from the initial to the final state. In the first stage of evolution, features develop in the profiles due to the linear instability of the initial profiles. These are secondary modulational instabilities, in contrast to the primary linear DW instabilities. Growth of these instabilities results in the formation of nonlinear features in the mean profiles, as well as in the turbulent PE profile. In the density profile these features are in the form of staircases; series of jumps (steepening) and steps (flattening) in the density profile. Simultaneously, the vorticity profile develops jagged (corrugated) features. These features are quasi-periodic with a characteristic length scale l_q.

Variable profiles evolve and transform through the local merger process. Merger of two jumps (steps) results in the formation of a wider jump (step) (see Fig. S1 in SM). The location of the jumps (steps) in n coincide with locations of maximum negative (positive) slope in u. Moreover, merger results in the increasing of the amplitude of the resulting shearing layer in the vorticity profile.

As a result of mergers, system scale size l_q grows and the profiles become smoother.

The process of mesoscale mergers gradually slows and stops. Although beyond this evolutionary time, and away from the boundaries, the profiles formed are locally stationary, they will evolve globally by profile migration. Migration refers to when density staircase and the shear lattice, detach and delocalize from their initial positions and migrate towards the boundaries. Migrating density barriers and shear layers condense as they reach the boundaries. This process continues until the steady macroscale density barrier and the shearing profile form. We should note that a pattern propagation was also advocated by Kosuga *et al* [31, 32], in an alternative theory approach to E × B shear layer pattern formation due to the propagation of heat-flux modulations. Figure 2 shows the density and shearing profile during the migration stage. In Fig.2a the density barriers move up the the density gradient in an "escalator"-like motion. Moreover, Fig.2b shows that along with the density profile, the shearing pattern also moves to the left and condenses at the boundary. Migration takes place over a much longer evolutionary time $\sim \mathcal{O}(10^4)$, in comparison to the earlier stages of evolution $\sim \mathcal{O}(10^2)$ (note that time is scaled to the external production timescale γ_ε^{-1}). Therefore, mesoscale features spend most of their lifetime migrating.
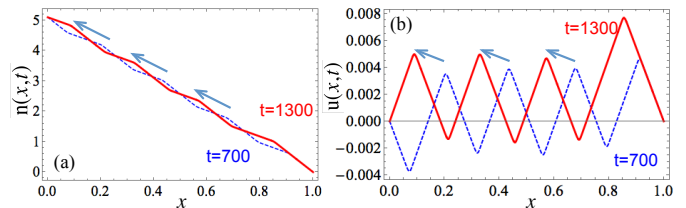

FIG. 2: (a)Upward, escalator-like migration of the step at times $t = 700$ and $t = 1300$. (b) Detachment of shearing pattern from the location of formation, and migration towards the boundary.

Spreading of turbulent PE is necessary in the formation of structures as it regulates the steepening in the ε profile. Lowering β results in the formation of more steps and jumps in the density profile (see Fig.S2 in SM). Moreover, below a value for β, the numerical solutions become too stiff to carry out, due to the fine spatial scale of instabilities and extreme local steepening of gradients. Raising β results in the formation of smaller number of jumps-steps in the staircase profiles. In the extreme case of large β, turbulent spreading of PE prevents the formation of any spatial structure in the mean fields.

c. Flux driven evolution: For the study of the global transport bifurcation of the steady macro-state we use the amplitude of an additional external particle flux drive, Γ_0, as the control parameter. The external source is taken to be sharply peaked on the axis with a constant width. For the initial condition of the density, the form
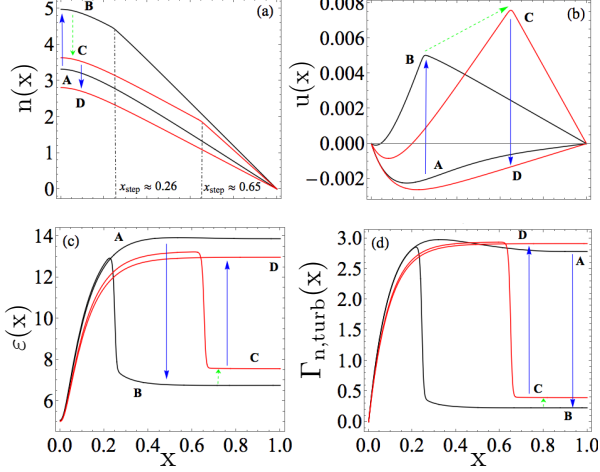
FIG. 3: Transformation in the profiles of (3a) density, (3b) vorticity, (3c) turbulent PE, and (3d) turbulent particle flux. Forward transition is from **A** to **B**, and backward transition is from **C** to **D**
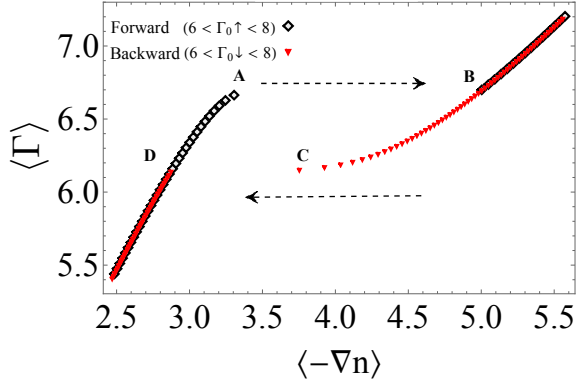

FIG. 4: Global particle flux versus density gradient, showing hysteresis behavior.

$n_0(x) = -g_i \left(x - 1 + \frac{1}{b} \left[e^{-bx} - e^{-b} \right] \right)$ is used $(b \gg 1)$. Away from $x = 0$, $\partial_x n_0$ is uniform and close to $-g_i$. The density equation including the flux drive is given by:

$$\partial_t n = -\partial_x \Gamma_{\text{tot}}; \quad \Gamma_{\text{tot}}(x,t) = \Gamma(x,t) + \Gamma_{\text{dr}}(x) \quad (6)$$

where $\Gamma(x,t) = -\left[\left(\frac{l^2 \varepsilon}{\alpha} \right) + D_c \right] \partial_x n$ is the sum of the turbulent and the collisional diffusion fluxes. As the solutions evolve to their final steady-state, Γ_{tot} saturates and becomes uniform. As Γ_0 is increased beyond a threshold of transition Γ_{th}, the steady macro-state of the system undergoes a transport bifurcation. As a result, the steady-state profiles of the n, u and ε undergo a drastic transformation. Fig.3 shows the transformation of the steady-state profiles as Γ_0 is raised from 6 to 8 and brought back down to 6, in one parameter scan run. Time

variation of Γ_0 is adiabatic, so that at all times the system is close to a steady-state solution, except for the short transition times.

Two different transitions can occur. The forward transition (FT) occurs for $\Gamma_0 = \Gamma_{\text{th}}^{\text{f}} \approx 7.39$, as Γ_0 is increasing, and backward transition (BT) occurs for $\Gamma_0 = \Gamma_{\text{th}}^{\text{b}} \approx 6.838$, as Γ_0 is decreasing. In Fig.3, curves labeled **A** and **B** are snapshots of the profiles for which Γ_0 is respectively, slightly below and slightly above $\Gamma_{\text{th}}^{\text{f}}$, i.e., $\Gamma_0|_{\mathbf{A}} \lesssim \Gamma_{\text{th}}^{\text{f}} \lesssim \Gamma_0|_{\mathbf{B}}$ (in the BT, $\Gamma_0|_{\mathbf{D}} \lesssim \Gamma_{\text{th}}^{\text{b}} \lesssim \Gamma_0|_{\mathbf{C}}$). During these fast transitions, the system is not in steady-state. For the FT (from **A** to **B**), Fig.3a shows the rise in n with the formation of macro-step and Fig.3c depicts the drop in ε level in the density jump region $x > 0.65$. Moreover, Fig.3d shows a drop in the turbulent particle flux beyond x_{step}, which implies that the steady macro-step acts as a *barrier* for the turbulent transport of particles. Furthermore, Fig.3b shows a sign reversal of u for **B** compared to **A** (except in the close vicinity of $x = 0$) along with the enhancement of its amplitude. The differences between the profiles for $\Gamma_0 > \Gamma_{\text{th}}^{\text{f}}$ and $\Gamma_0 < \Gamma_{\text{th}}^{\text{f}}$, lead us to define the former as the enhanced confinement (EC) modes and the latter as the normal confinement (NC) modes. In the BT, the system transitions from the EC mode (**C**) to the NC mode (**D**). In this fast process, the barrier position x_{step} moves from $x \approx 0.65$ to the right boundary at $x = 1$, as the height of the barrier decreases to zero.

In order to elucidate the physics of hysteresis in the process described above, the *global* particle flux-density gradient relation of the steady-states is mapped in Fig.4. The vertical and the horizontal axes are respectively $\langle \Gamma \rangle$ and $\langle -\partial_x n \rangle$, where $\langle \rangle$ is averaging over the spatial dimension. Data points shown with diamonds (triangles) are the $(\langle -\partial_x n \rangle, \langle \Gamma \rangle)$ values of the system as Γ_0 increases (decreases). Critical transition points are shown in Fig. 4. The **A** - **B**, and **C** - **D** gaps result from the transport bifurcation, leading, respectively, to barrier formation in the FT, and barrier annihilation in BT. The loop formed due to the separation between the FT and the BT, results from transport bifurcation taking place at different values of Γ_{th} in each direction. This loop is a clear depiction of hysteresis behavior in this process.

In summary, this reduced analytical model manifests emergence of quasi-periodic mesoscale density staircase structures, colocated with a lattice of shears. These meso structures reorganize and evolve through merger and spatial migration, and so form a *macro* steady-state. Some turbulent spreading is necessary to the formation of structures as it regulates the steepening of the turbulent PE. *The macro-state of a system driven by an external particle flux undergoes a global transport bifurcation*, from a normal confinement state to an enhanced confinement state, as the amplitude of the flux drive is increased beyond a threshold of transition. This transition is identified by the transformation of the system profiles: formation of a step-jump structure with the rise in overall level in the density profile n, a regional drop in the

level of turbulent PE and turbulent particle flux, sign reversal and amplitude enhancement of the shearing profile u. Furthermore, the system exhibits hysteresis between the forward and backward transition of the macro-state.

[1] R. W. Schmitt, Ann. Rev. Fluid Mech. **26**, 255 (1994).
[2] J. S. Turner, "Buoyancy effects in fluids," (Cambridge University Press., 1973).
[3] W. J. Merryfield, J. Phys. Ocean. **30**, 1046 (1999).
[4] T. Radko, J. Fluid Mech. **497**, 365 (2010).
[5] P. S. Marcus, Annu. Rev. Astron. Astrophys. **31**, 523 (1993).
[6] R. Wood and M. McIntyre, J. Atmos. Sci **67**, 1261 (2010).
[7] P. Diamond, S. Champeaux, M. Malkov, A. Das, I. Gruzinov, M. Rosenbluth, C. Holland, B. Wecht, A. Smolyakov, Z. Lin, and T. Hahm, Nucl. Fusion **41**, 1067 (2001).
[8] A. M. Dimits, T. J. Williams, J. A. Byers, and B. I. Cohen, Science **77**, 71 (1996).
[9] Z. Lin, T. Hahm, W. Lee, W. Tang, and R. White, Science **281**, 1835 (1998).
[10] P. H. Diamond, S.-I. Itoh, K. Itoh, and T. S. Hahm, Plasma Phys. Control Fusion **47**, R35 (2005).
[11] P. H. Diamond, A. Hasegawa, and K. Mima, Plasma Phys. Control. Fusion **53**, 124001 (2001).
[12] G. Dif-Pradalier, P. H. Diamond, V. Grandgirard, Y. Sarazin, J. Abiteboul, X. Garbet, P. Ghendrih, A. Strugarek, S. Ku, and C. S. Chang, Phys. Rev. E **82**, 025401(R) (2010).
[13] G. Dif-Pradalier, G. Hornung, P. Ghendrih, Y. Sarazin, F. Clairet, L. Vermare, P.H. Diamond, J. Abiteboul, T. Cartier-Michaud, C. Ehrlacher, D. Esteve, X. Garbet, V. Grandgirard, Ö. D. Gürcan, P. Hennequin, Y. Kosuga, G. Latu, P. Maget, P. Morel, C. Norscini, R. Sabot, and A. .Storelli, Phys. Rev. Lett. **114**, 085004 (2015).
[14] Y. Sarazin, X. Garbet, P. Ghendrih, and S. Benkadda, Phys. of Plasmas **7**, 1085 (2000).
[15] X. Garbet, Y. Sarazin, F. Imbeaux, P. Ghendrih, C. Bourdelle, . D. Grcan, and P. H. Diamond, Phys. of Plasmas **14**, 122305 (2007).
[16] Y. Idomura, H. Urano, N. Aiba, and S. Tokuda, Nucl. Fusion **49** (2009).

[17] E. Kim and P. H. Diamond, Phys. Plasmas **9** (2002).
[18] B. N. Rogers, W. Dorland, and M. Kotschenreuther, Phys. Rev. Lett. **85**, 5336 (2000).
[19] S. Kobayashi and B. N. Rogers, Phys. Plasmas **19**, 012315 (2012).
[20] L. D. Landau, E. M. Lifshitz, A. M. Kosevich, and L. P. Pitaevskii, "Theory of elasticity," (Elsevier, 1986).
[21] O. M. Phillips, Deep-Sea Res. **19**, 79 (1972).
[22] M. N. Juckes and M. E. McIntyre, Nature **328**, 590 (1987).
[23] N. J. Balmforth, S. G. Llewellen-Smith, and W. R. Young, J. Fluid Mech. **335**, 329 (1998).
[24] A. Hasegawa and M. Wakatani , Phys. Rev. Lett. **59**, 1581 (1987).
[25] M. Wakatani and A. Hasegawa, Phys. Fluids **27**, 3 (1984).
[26] A. Ashourvan, P. H. Diamond, and Ö. D. Gürcan, Phys. Plasmas **22**, 050704 (2015).
[27] K. H. Burell, Phys. of Plasmas **4**, 1499 (1997).
[28] H. Biglari, P. H. Diamond, and P. W. Terry, Phys. Fluids B **2** (1990).
[29] T. S. Hahm, P. H. Diamond, Z. Lin, K. Itoh, and S.-I. Itoh, Plasma Phys. Control.Fusion **46**, A323 (2004).
[30] P. B. Rhines, J. Fluid Mech. **69**, 417 (1975).
[31] Y. Kosuga, P. H. Diamond, and Ö. D. Gürcan, Phs. Rev. Lett. **110**, 105002 (2013).
[32] Y. Kosuga, P. H. Diamond, G. Dif-Pradalier, and Ö. D. Gürcan, Phys. of Plasmas **21**, 055701 (2014).
[33] N. T. Howard, C. Holland, A. E. White, M. Greenwald, and J. Candy, Nucl. Fusion **56**, 014004 (2016).
[34] See Supplemental Material at [URL], for details on constructing the reduced model, Fig. S1: merger between steps and jumps, Fig. S2: dependence of the number of formed steps on the strength of turbulence spreading, and Fig. S3: flux gradient landscape.